Engineering 3 (2017) 806–816

Contents lists available at ScienceDirect

Engineering

journal homepage: www.elsevier.com/locate/eng

Research
Bridge Engineering—Article

Mechanical Behavior of a Partially Encased Composite Girder with Corrugated Steel Web: Interaction of Shear and Bending

Jun He [a,*], Sihao Wang [b], Yuqing Liu [b], Zhan Lyu [c], Chuanxi Li [a]

[a] School of Civil Engineering, Changsha University of Science and Technology, Changsha 410114, China
[b] Department of Bridge Engineering, Tongji University, Shanghai 200092, China
[c] Department of Civil and Environmental Engineering, Imperial College London, London SW7 2AZ, UK

ARTICLE INFO

Article history:
Received 25 March 2017
Revised 3 June 2017
Accepted 26 November 2017
Available online 26 December 2017

Keywords:
Encased concrete
Composite girder
Corrugated steel web
Interaction of shear and bending

ABSTRACT

The synergistic use of partially encased concrete and composite girders with corrugated steel webs (CGCSWs) has been proposed to avoid the buckling of corrugated steel webs and compression steel flanges under large combined shear force and bending moment in the hogging area. First, model tests were carried out on two specimens with different shear spans to investigate the mechanical behavior, including the load-carrying capacity, failure modes, flexural and shear stress distribution, and development of concrete cracking. Experimental results show that the interaction of shear force and bending moment causes the failure of specimens. The bending-to-shear ratio does not affect the shear stiffness of a composite girder in the elastic stage when concrete cracking does not exist, but significantly influences the shear stiffness after concrete cracking. In addition, composite sections in the elastic stage satisfy the assumption of the plane section under combined shear force and bending moment. However, after concrete cracking in the tension field, the normal stresses of a corrugated web in the tension area become small due to the "accordion effect," with almost zero stress at the flat panels but recognizable stress at the inclined panels. Second, three-dimensional finite-element (FE) models considering material and geometric nonlinearity were built and validated by experiments, and parametric analyses were conducted on composite girders with different lengths and heights to determine their load-carrying capacity when subjected to combined loads. Finally, an interaction formula with respect to shear and flexural strength is offered on the basis of experimental and numerical results in order to evaluate the load-carrying capacity of such composite structures, thereby providing a reference for the design of partially encased composite girders with corrugated steel webs (PECGCSWs) under combined flexural and shear loads.

© 2017 THE AUTHORS. Published by Elsevier LTD on behalf of Chinese Academy of Engineering and Higher Education Press Limited Company. This is an open access article under the CC BY-NC-ND license (http://creativecommons.org/licenses/by-nc-nd/4.0/).

1. Introduction

Composite girders with corrugated steel webs (CGCSWs), as shown in Fig. 1, which include prestressed concrete slabs, corrugated steel webs, or internal or external tendons, have been applied to highway and railway bridges as a promising steel-concrete hybrid structure. No restraint exists between the slabs and webs due to the use of corrugated steel webs, which can alleviate structural responses due to shrinkage, creep of concrete, and temperature differences between slabs and webs. The "accordion effect" of corrugated webs efficiently introduces prestressing into the concrete slabs, while the combination of concrete slabs and corrugated steel webs improves the structures' strength, stability, and material efficiency [1–3].

Since the construction of the first highway bridge using corrugated webs, which occurred in France in 1986 (Cognac Bridge), numerous composite bridges with corrugated steel webs have been erected around the world [2–4]. In addition, a considerable number of experimental and theoretical studies have been carried out on such bridges, including studies on their bending behavior [5–15], shear behavior [16–24], torsional behavior [25–27], and dynamic behavior [28,29].

Experimental, numerical, and theoretical studies have been carried out by Elgaaly et al. [5], Huang et al. [6], and Oh et al. [7] on the "accordion effect" of steel girders with corrugated webs. Due to this effect, the corrugated steel web makes almost no contribution to the section flexural strength. Thus, the ultimate bending

* Corresponding author.
E-mail address: frankhejun@163.com (J. He).

https://doi.org/10.1016/j.eng.2017.11.005
2095-8099/© 2017 THE AUTHORS. Published by Elsevier LTD on behalf of Chinese Academy of Engineering and Higher Education Press Limited Company.
This is an open access article under the CC BY-NC-ND license (http://creativecommons.org/licenses/by-nc-nd/4.0/).

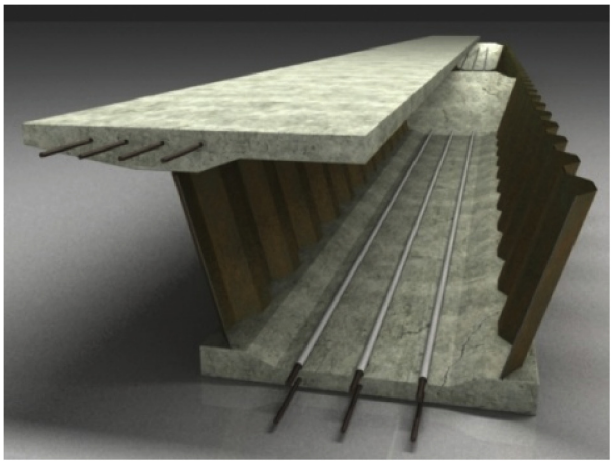

Fig. 1. Layout of a CGCSW.

moment capacity of the girder depends on the flange yield strength [5,8–11]. This conclusion was found to be applicable to composite girders after several investigations on the flexural capacity of CGCSWs [12–15].

The shear behavior and shear bucking of corrugated steel webs have been extensively studied both experimentally and theoretically, and the results show that corrugated steel webs can resist almost all of the shear forces [16,17]. Therefore, the effective shear modulus of the corrugated steel web, which is determined while taking the shear deformation and web corrugation into account, is a key parameter in predicting the shear force resistance accurately [9]. Moreover, the shear yielding of the corrugated steel web and the buckling properties, including global buckling, local buckling, and interactive buckling, controls the calculation of shear strength [18–21]. Based on experimental results on the shear performance of steel or composite girders with corrugated steel webs in Europe, the United States, and Asia, an assessment of predicted equations was conducted [22]. It was found that the elastic global or local buckling equations overestimate the shear strength. Considering material nonlinearity, residual stress, and initial geometric imperfections, inelastic equations for shear stress were provided in design codes [23,24].

Results from previous studies show that the shear force and bending moment are resisted by the corrugated steel webs and by flanges, respectively; no interaction takes place between the global flexure and the shear behavior of these girders [5,16]. However, Kuchta [30] investigated the mechanical performance of steel girders with corrugated steel webs subjected to combined shear force and bending moment. The results showed that there is a small reduction in the load-carrying capacity under combined loads, with a maximum reduction of 8.33% due to the interaction of shear and bending.

According to data from the design and construction of composite bridges with corrugated steel webs in China and Japan, continuous girders and rigid frames, which were used for about 80% of such bridges, are the two most popular typologies. However, the large shear force and bending moment caused by the hogging moment at the intermediate supports can lead to cracking on the concrete upper slab. After concrete cracking, the steel reinforcements in the tensile concrete slab resist tensile stress, whereas the lower parts of the webs and bottom flanges are vulnerable to lateral-torsional buckling resulting from the large compressive stress. In addition, local failure was observed in the vicinity of the diaphragms of specimens tested by Kosa et al. [31], Shitou et al. [32], and Chen [33] due to the interaction between web shear deformation and local bending of concrete slabs [33]. Thus, the middle support area is the weak area, having low durability and strength. Therefore, as shown in Fig. 2, concrete encasement in this area has been proposed in order to improve the structural performance, especially for structures with a large section depth. This concrete encasement, which is surrounded by corrugated steel webs and the upper and lower flanges, is expected to enhance the structural bending, shear strengths, and buckling resistance of the corrugated steel webs. Moreover, the shear stiffness of the encased corrugated steel web in the vicinity of the diaphragms is much larger than that of a pure corrugated steel web, so the concrete encasement greatly relieves the interaction between web shear deformation and the local bending of concrete slabs.

Few recent reports exist on design provisions for the partially encased composite girder with corrugated steel web (PECGCSW). We tested the flexural and shear behaviors of I-shaped steel and composite girders with a flat or corrugated web by means of parametric studies. These parameters include the thickness of the steel web and the level of composite action between the steel web and the encased concrete. Through comparison with experimental results, theoretical and numerical models were built and validated in order to predict the flexural and shear strength [34–36]. When the encased concrete was connected to the corrugated steel web by shear connectors, it was shown that the mechanical behavior of such a composite girder was totally different from that of a steel girder with a corrugated web under individual flexural or shear loading. However, PECGCSWs are recommended for application in the region of the intermediate supports of a continuous bridge, where a large shear force and bending moment exist. Referring to the continuous bridge, it is necessary to understand the mechanical performance of PECGCSWs under a combined shear force and bending moment. In addition, the interaction of the shear force and bending moment on a PECGCSW is different from that on a steel girder with a corrugated web, and has not yet been sufficiently studied.

This paper aims to understand the mechanical behavior of a PECGCSW that is subjected to combined loadings of shear and bending by means of model tests and numerical analyses. Two encased corrugated steel web girders with different ratios of bending moment to shear force were tested in order to investigate their load-carrying capacity and failure mechanism. Next, numerical finite-element (FE) models of test specimens that incorporated material and geometric nonlinearity were built and validated by experimental results. Parametric analyses were carried out using calibrated FE models in order to investigate the interaction of flexural and shear strength. On the basis of these experimental and numerical results, this paper proposes an interaction formula for the shear and flexural strength to assess the load-carrying capacity of such composite girders.

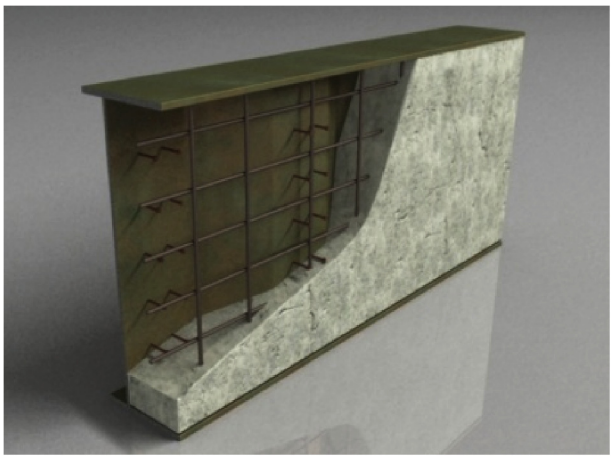

Fig. 2. Structural details of the PECGCSW.

2. Experimental program

2.1. Experimental specimens

In order to investigate the mechanical behaviors of PECGCSWs that were subjected to combined loadings, two I-shaped composite girders, referred to here as SBC1 and SBC2, were prepared and tested. The total length and height of the experimental specimens were 2.26 m and 0.54 m, respectively. These specimens contained one corrugated steel web with a depth of 500 mm and a thickness of 8 mm, and two steel flanges, each with a width of 300 mm and a thickness of 20 mm.

Each specimen was divided into two areas: the test area, with a length of L_1, and the reinforced area, with a length of L_2. The latter was strengthened by extra steel stiffeners in order to avoid failure in this area. Fig. 3 shows the structural details of the experimental specimens. The lengths of L_1 and L_2 were 710 mm and 990 mm, respectively, for SBC1, and 990 mm and 710 mm, respectively, for SBC2. As depicted in Fig. 3(d), the unit wavelength of the corrugated steel web was 560 mm; the flat and inclined panel was 150 mm wide, while the projected width for the inclined panel was 130 mm.

The encased concrete was fully connected to the corrugated steel web by means of welded shear studs, each with a height of 80 mm and a diameter of 16 mm. The 8 mm diameter reinforcing bars (D = 8 mm) were distributed horizontally and vertically in the encased concrete, and each end of these reinforcing bars was welded onto the stiffeners or the flanges.

The fabrication process of the test specimens was the same as that of previous shear test specimens [34]: First, the steel girder was laid flat; next, concrete was cast on the top side of the flat girder. In order to facilitate concrete casting and enhance concrete confinement, intermediate and side stiffeners were arranged at the steel girders before concrete construction.

2.2. Material properties

Table 1 summarizes the material properties of the concrete, and includes the compressive strength, tensile strength, and Young's modulus that were obtained from material tests on concrete cubes 28 days after casting. Table 2 provides the material properties of the steel, including the yielding strength, tensile strength, elongation, and Young's modulus from material test samples cut from the steel flange, the corrugated steel web, and the steel reinforcement of the composite girders.

2.3. Loading process and measuring arrangement

Loading tests were conducted on the mechanical performance of a PECGCSW under combined flexural and shear loads. As shown in Fig. 4, the test specimen was simply supported with a clear span of 1830 mm, and a concentrated load was applied at the interaction section between the test area and the reinforced area using a 10 000 kN servo loading system.

Preloading was implemented to check the testing equipment for the following conditions: ① a good boundary condition between the servo loading system and the specimens, and between the supporting bearings and the specimens; ② the reliability of the experimental equipment; and ③ the work performance of the measuring instruments. Next, a concentrated load was applied to the specimens at two stages: In the first stage, the load increased by increments of 2 $kN \cdot s^{-1}$ until the yield of the steel flange, using the force control method; in the second stage, vertical displacement was applied with a speed of 0.0067 $mm \cdot s^{-1}$ until structural failure, using the displacement control method.

The deflection at the loading point and at the middle section of the test area (Section 1-1) was measured by linear variable differential transformer (LVDT). The strain states at Section 1-1 were measured by strain gauges mounted on the surface of the concrete encasement, steel plates, and reinforcements. In addition, the initiation and propagation of concrete cracking, as well as the development of crack length and width, were observed and recorded during the loading process. Data from all the instruments, including the LVDTs, stain gauges, and load transducers, were automatically recorded at regular intervals during the load test.

3. Experimental results and discussion

3.1. Load-carrying capacity and failure modes

Fig. 5 illustrates the relationship between the section shear force and the vertical displacement at Section 1-1 until the failure

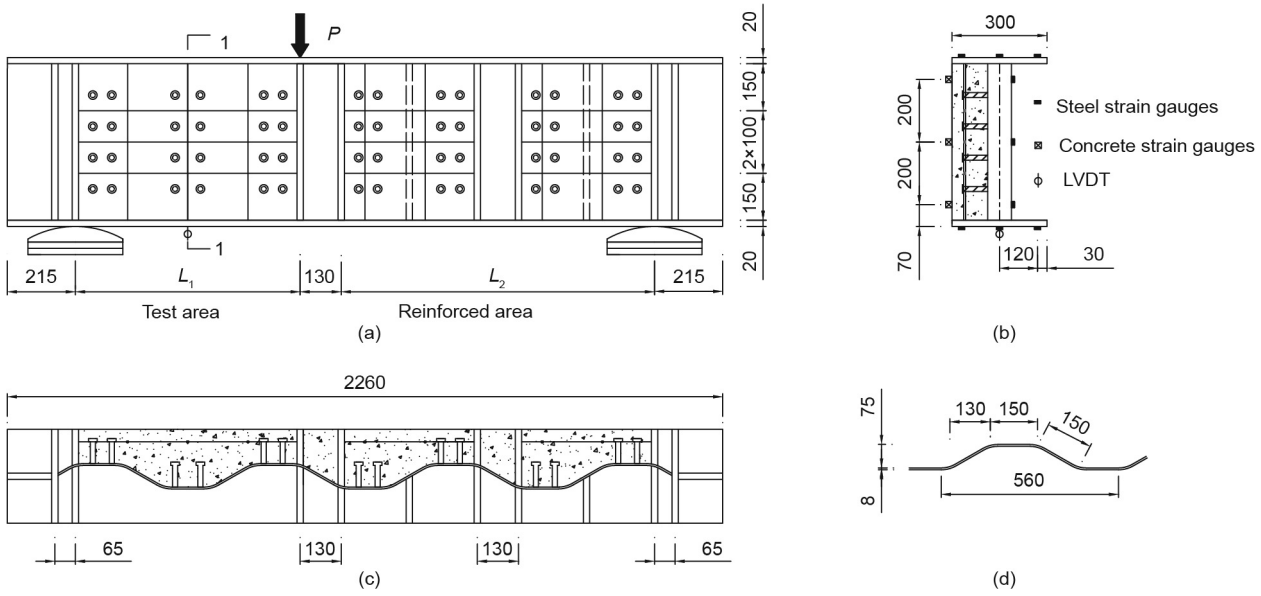

Fig. 3. Structural details of the experimental specimens SBC1 and SBC2 (unit: mm). (a) Elevation layout; (b) cross-section; (c) plane layout; (d) corrugation profile. LVDT: linear variable differential transformer.

Table 1
Material properties of the concrete.

Nominal strength (MPa)	Compressive strength (MPa)		Tensile strength (MPa)		Young's modulus (MPa)	
	Sample value	Average value	Sample value	Average value	Sample value	Average value
50	51.9	54.5	3.62	3.78	5.03×10^4	4.94×10^4
	54.5		3.78		4.79×10^4	
	57.1		3.95		4.99×10^4	

Table 2
Material properties of the steel.

Component	Yielding strength (MPa)	Tensile strength (MPa)	Elongation (%)	Young's modulus (MPa)
Web (8 mm)	386	488	31	2.00×10^5
Flange and stiffener (20 mm)	384	460	40	1.99×10^5
Reinforcing bar (D = 8 mm)	342	556	34	1.96×10^5

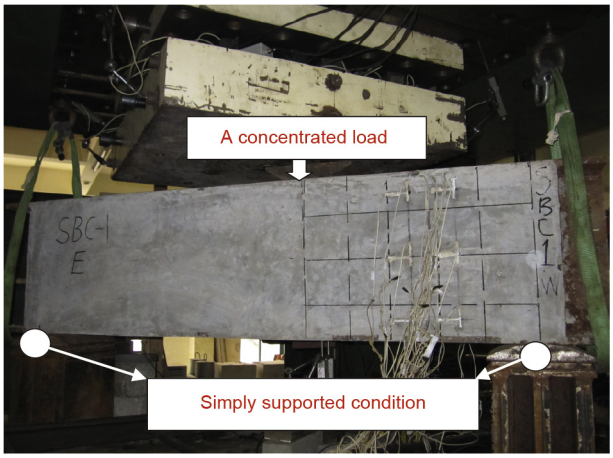

Fig. 4. Test setup and loading system.

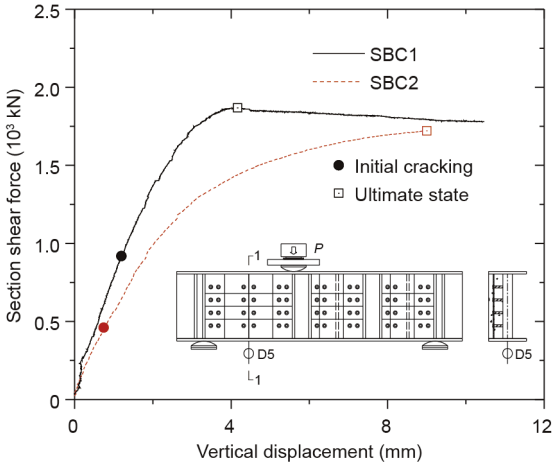

Fig. 5. The relationship between the section shear force and the vertical displacement at Section 1-1.

of the test specimens. For both test specimens SBC1 and SBC2, the deflection increases linearly with the increase of section shear force before concrete cracking, and then enters into a nonlinear state after concrete cracking. For specimen SBC1, the value of the section shear force drops slowly after its peak, but the vertical displacement still increases. For specimen SBC2, the section shear force increases gradually until the ultimate state, and remains nearly constant afterward with a large deflection, showing high ductility.

Table 3 lists the experimental results, including the sectional shear stiffness (at Section 1-1) before and after concrete cracking, which are defined as K_{s1} and K_{s2}, respectively; the bending moment M, the shear force V, the deflection δ, and the shear rotation γ at the initial cracking state (M_2, V_2, δ_2, γ_2) and at the ultimate state (M_3, V_3, δ_3, γ_3). The shear stiffness is calculated as the ratio of the section shear force increment (ΔV) to the shear rotation increment ($\Delta\gamma$) at the test area.

As the bending-to-shear ratio, R ($R = M/V$), increases from 0.355 (SBC1) to 0.495 (SBC2), the shear stiffness K_{s1} shows only a slight difference, whereas the shear stiffness K_{s2} decreases by more than 10%. The shear force in SBC2 at the initial cracking state is almost half of that in SBC1. At the ultimate state, in comparison with SBC1, the bending moment in SBC2 increases by approximately 30%, whereas the shear force decreases by about 10%. The ultimate deflection of SBC2 increases twice, showing better ductility. In addition, the shear stiffness K_{s2} of SBC2 decreases more obviously than that of SBC1, before and after concrete cracking.

The failure modes of specimens SBC1 and SBC2 are described in Fig. 6. Both specimens show obvious coupled flexural and shear failure caused by the interaction of combined loads. Flexural and shear cracking were observed on the surface of the concrete. Shear cracking plays a controlling role for SBC1, but flexural cracking plays that role for SBC2.

3.2. Crack development

Fig. 7 shows the crack initiation and development process on the concrete at the test area for specimens SBC1 and SBC2. For specimen SBC1, two initial cracks occurred under a load of 1500 kN, involving one shear crack and one flexural crack. With the increase of the applied load, the shear crack propagated and distributed; however, the flexural crack did not significantly propagate. At the ultimate state, the width of the main crack (i.e., the shear crack) and of the nearby parallel cracks increased quickly. The encased concrete finally failed following the formation of tensile and compressive struts, indicating that shear cracks control the failure mode. For specimen SBC2, one initial flexural crack occurred under a load of about 1000 kN; afterward, this flexural crack propagated and a second flexural crack occurred under a load of about 2000 kN. Typical shear cracks appeared when the load increased to 2500 kN. Flexural and shear cracks then continued to propagate until the ultimate state. Both flexural and shear cracks controlled the final failure mode.

Fig. 8 describes the crack width development of the initial crack for specimens SBC1 and SBC2 until failure. The crack width increased to 0.5 mm in an approximately linear fashion as the load was applied up to 2500 kN, and then increased rapidly until failure

Table 3
Test results of specimens.

Specimens	R	K_{s1} (kN·rad^{-1})	K_{s2} (kN·rad^{-1})	Initial cracking state				Ultimate state			
				M_2 (kN·m)	V_2 (kN)	δ_2 (mm)	γ_2 (10^{-3} rad)	M_3 (kN·m)	V_3 (kN)	δ_3 (mm)	γ_3 (10^{-3} rad)
SBC1	0.355	240 977	215 552	325.8	917.8	1.2	3.38	663.3	1 868.4	4.2	11.83
SBC2	0.495	259 782	190 474	227.4	459.5	0.7	1.41	851.7	1 720.6	9.0	18.18

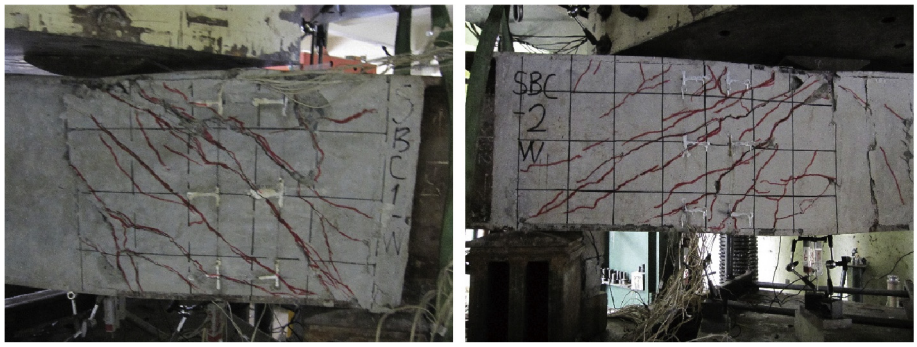

Fig. 6. The failure modes of the test specimens. (a) SBC1; (b) SBC2.

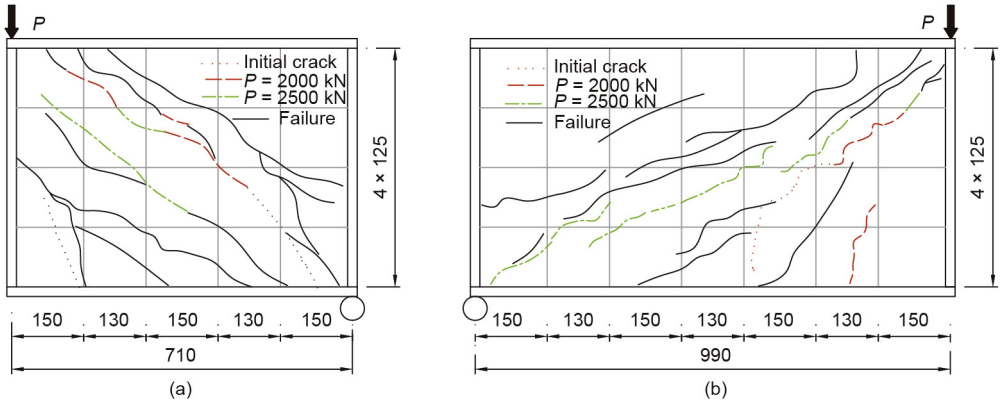

Fig. 7. Crack initiation and development process on the concrete at the test area (unit: mm). (a) SBC1; (b) SBC2.

due to steel yielding and the redistribution of internal force. The final crack width was 3 mm for specimen SBC1 and 5 mm for specimen SBC2.

3.3. Strain distributions

Fig. 9 illustrates the distribution of normal strain along the height of the steel girder at Section 1-1 during the loading process. It should be noted that the measured section for specimen SBC1 was at the corrugated steel web with a flat panel, whereas the corresponding section for specimen SBC2 was at the corrugated steel web with an inclined panel.

The top steel flange was in compression while the bottom steel flange was in tension. The normal strains were distributed uniformly along the flange width when the applied load was less than the cracking load; as the applied load increased, the normal strain distribution became uneven, and the strain of the flange within the concrete side was larger than that of the other side without concrete.

Under the combined loads of the shear force and bending moment, the corrugated steel web was in compression and the strain was vertically distributed in an approximately linear fashion

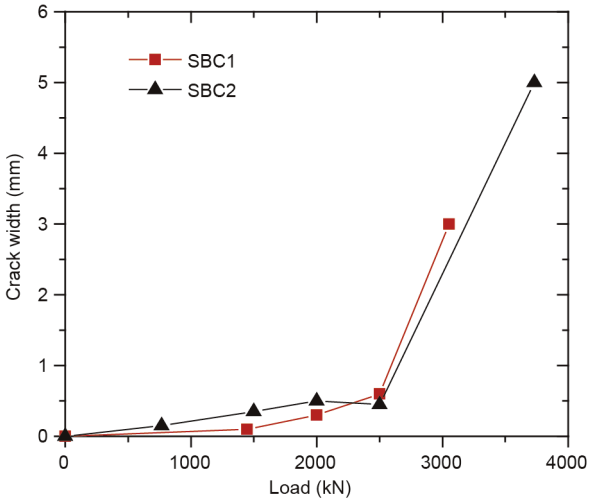

Fig. 8. The relationship between load and crack width.

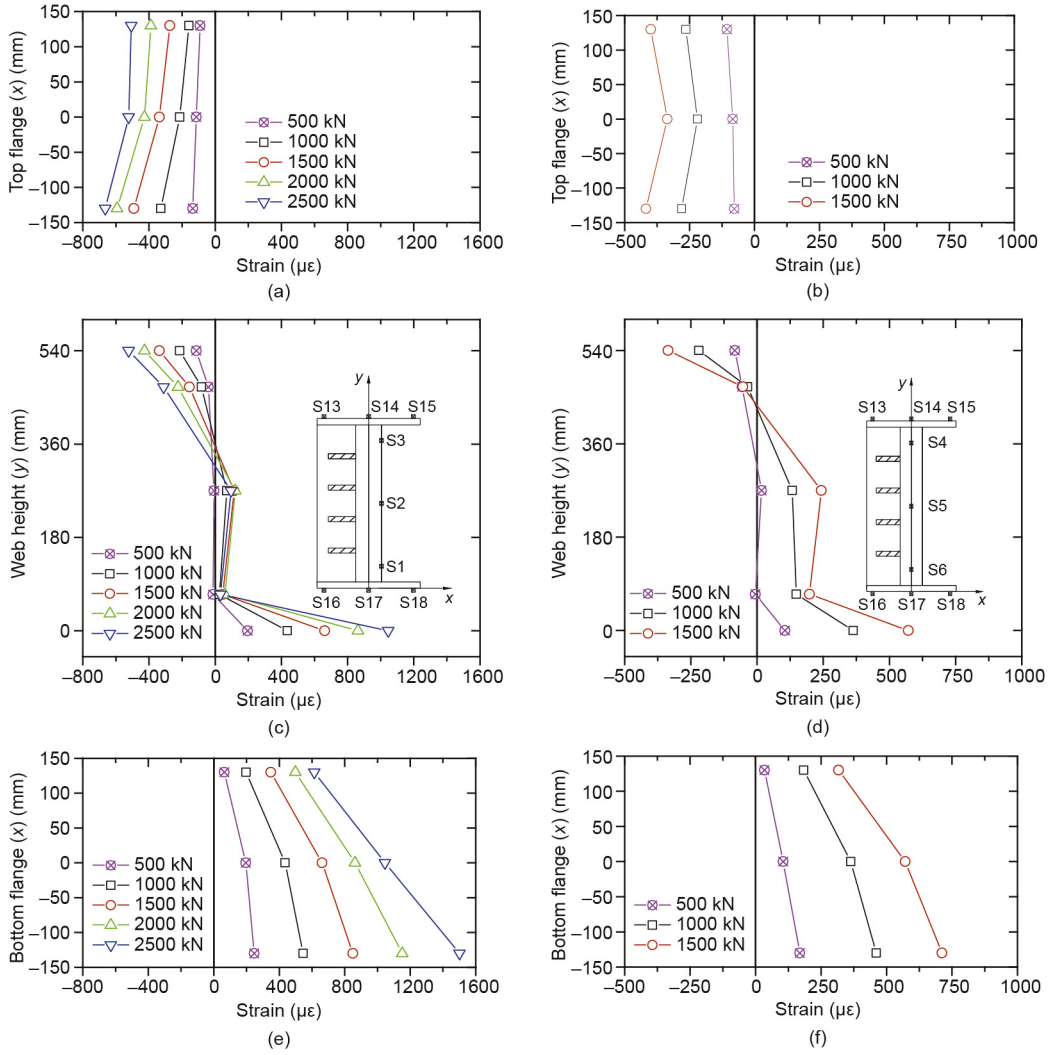

Fig. 9. The distribution of normal strain along the height of the steel girder at Section 1-1. (a) Top flange of SBC1; (b) top flange of SBC2; (c) corrugated steel web of SBC1; (d) corrugated steel web of SBC2; (e) bottom flange of SBC1; (f) bottom flange of SBC2.

from the top flange to the natural axis. However, the bottom part of the web was in tension where the concrete was vulnerable to cracking. After concrete cracking in this part, the normal strain of the corrugated steel web was very small due to the "accordion effect," and there was less longitudinal constraint from the cracked concrete. Therefore, the contribution to flexural capacity from the tension part of the web can be neglected. In addition, the normal strains of the steel web at the tension part were larger for SBC2 than for SBC1, because the inclined panel for SBC2 resisted more restraint from the encased concrete than the flat panel for SBC1 did.

Similarly, the distribution of normal strain along the height of the encased concrete at Section 1-1 during the loading process is shown in Fig. 10. There were no cracks on the surface of the concrete in the elastic stage, when the applied load was smaller than 500 kN, so it is accepted that the sectional strain distribution agrees with the assumption of the plane section. Under the ultimate load, the concrete almost cracked below the neutral axis and the maximum cracking width was larger than 3 mm; the compressive strains of the concrete remained almost the same above the neutral axis, especially near the top flange.

4. Finite-element model

A three-dimensional model of the experimental specimen was established using the general FE software (ANSYS 11.0), taking material and geometric nonlinearity into account, as shown in Fig. 11. The concrete components, steel plates, reinforcements, and shear studs were simulated using solid elements (SOLID65), shell elements (SHELL93), link elements (LINK8), and spring elements (COMBIN39), respectively. Perfect bond condition was assumed between the reinforcing bars and the concrete. However, in order to account for composite action between the corrugated steel web and the surrounding concrete, contact elements were adopted in the FE model to consider the adhesion bonding of the interface between the steel and concrete. The PECGCSW was simply supported and was subjected to a concentrated load, which was simulated under the same conditions as the experimental tests.

Three-dimensional solid elements with eight nodes (SOLID65) were adopted to simulate the encased concrete. These elements contained a smeared crack model for concrete cracking in the tension area and a plasticity model for concrete crushing in the compression area. In the compression part of the concrete, a traditional

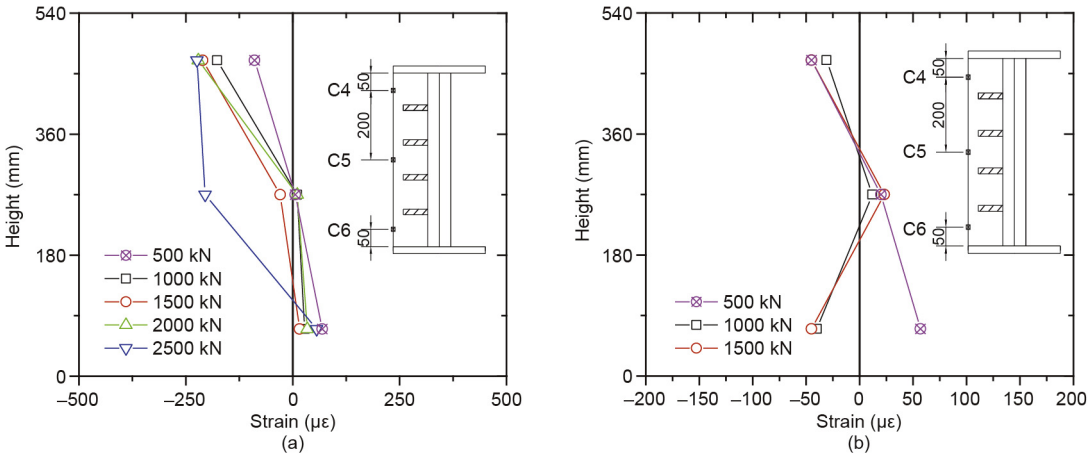

Fig. 10. The distribution of normal strain along the height of the encased concrete at Section 1-1. (a) SBC1; (b) SBC2.

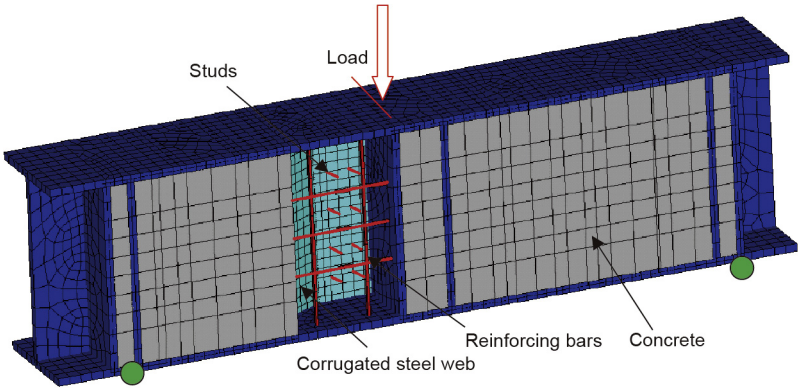

Fig. 11. FE model of the experimental specimen.

Hognestad model was used to express the stress-strain constitutive relation and was realized by the multi-linear isotropic hardening (MISO) option. The stress (f_c) versus strain (ε_c) of the compressive concrete was assumed to be a parabolic curve in the ascending stage for stress less than the concrete compressive strength f'_c, and was then keep constant, as follows:

$$\begin{cases} f_c = f'_c\left[2\left(\frac{\varepsilon_c}{\varepsilon'_c}\right) - \left(\frac{\varepsilon_c}{\varepsilon'_c}\right)^2\right] & \varepsilon_c \leqslant \varepsilon'_c \\ f_c = f'_c & \varepsilon'_c < \varepsilon_c \leqslant \varepsilon_{cu} \end{cases} \quad (1)$$

where ε_c and f_c are the concrete compressive strain and stress, respectively; and ε'_c is the compressive strain corresponding to f'_c. The ultimate compressive strain of the concrete, ε_{cu}, is assumed to be 0.004 in order to consider the confined effect of the encased concrete.

Regarding the concrete in tension, the tensile stress (f_t) versus strain (ε_t) relationship was depicted using a linear model in the ascending section when the stress was less than the crack resistance strength (f_{tr}). After that, the stress rapidly decreased to zero in a linear fashion until the ultimate tensile strain (ε_{tu}), taking into account the concrete softening, as expressed by the following equations:

$$\begin{cases} f_t = E_c\varepsilon_t \leqslant f_{tr} & \varepsilon_t \leqslant \varepsilon_{tr} \\ f_t = f_{tr}\left(1 - \frac{\varepsilon_t - \varepsilon_{tr}}{\varepsilon_{tu} - \varepsilon_{tr}}\right) & \varepsilon_{tr} < \varepsilon_t \leqslant \varepsilon_{tu} \\ f_{tr} = 0.23 f'^{2/3}_c \end{cases} \quad (2)$$

where E_c is Young's modulus of the concrete.

The steel components, including the steel flanges and the corrugated steel web, were modeled by shell elements (SHELL93), while the reinforcements were simulated by three-dimensional link elements (LINK8). An elastic-perfectly-plastic model was used to express the relation between strain and stress for the steel plate and reinforcements, and was realized by the bilinear kinematic hardening (BKIN) option in the FE model. In the plastic range, isotropic yielding was defined using the von Mises yield criterion. The reinforcements and surrounded concrete were assumed to be perfectly bonded together, and were simulated by sharing the nodes of the concrete element and the reinforcement element at the same position, while ignoring the relative slip between them.

The shear studs connecting the corrugated steel web and the encased concrete were modeled by nonlinear spring elements (COMBIN39). The constitutive model of the shear-slip relation for the spring elements was provided by Eq. (3) as recommended by Ollgaard et al. [37], where the ultimate shear force (Q_u) of the stud connectors was stipulated by the American Association of State Highway and Transportation Officials (AASHTO)'s load and resistance factor design (LRFD) specification [38], as shown in Eq. (4).

$$Q = Q_u\left(1 - e^{-0.7S}\right)^{0.4} \quad (3)$$

$$Q_u = \Phi 0.5 A_s\sqrt{f'_c E_c} \leqslant \Phi A_s F_u \quad (4)$$

where S is the relative slip of the shear studs; A_s is the area of the shear stud cross-section; F_u is the allowed minimum tensile strength of a shear stud; E_c is Young's modulus of the concrete; f'_c

is the concrete compressive strength; and Φ is the shear resistance factor of the stud connectors, which is set to 0.85.

The above FE model was adopted to predict the load-carrying capacity of the PECGCSWs under the combined loads of shear force and bending moment. The load (P)-deflection (δ) relationships of each specimen, which were measured from tests and simulated by FE methods, are shown in Fig. 12, in which P is a concentrated load applied on the test specimen and δ is the maximum deflection on the bottom flange at the loading point. The load-deflection curves in the elastic region from numerical simulation agree well with those from the experimental results. In the elastoplastic stage, steel yielding and concrete cracking or crushing result in nonlinearity of the load-deflection curve. There is no descending section in the simulated load-deflection curve, which is different from the experimental curve, since force control was used as the loading method in the numerical model. Moreover, after steel yielding, the stiffness of the FE model is slightly smaller than that of the test girder for SBC1. However, the ratios for SBC1 and SBC2 of the ultimate load obtained from FE analysis to the ultimate load obtained from tests are 0.98 and 0.96, respectively, indicating that the established FE models can be used to predict the load-carrying capacity behavior efficiently. The FE models of the PECGCSWs under separate shear force or bending moment were verified by our previous work [35,36].

5. Analytical study

5.1. Flexural strength

A multi-layer model has been proposed to predict the flexural strength of a PECGCSW, in which the steel girder and concrete encasement are divided into several layers. Fig. 13 shows the cross-section, sectional strain, and stress distribution of the multi-layer model in the vertical direction under the ultimate state, in which, b_f and t_f are the width and thickness of the steel flange, respectively; t_c is the width of the encased concrete; h is the total height of the composite girder; d'_s and d_{st} are the distance from the compressive and tensile reinforcement to the top fiber, respectively; $d_{w,i}$ is the distance from the ith layer of web to the top fiber; ε_{tf} and ε_{bf} are the strain of the top and bottom flange, respectively; and $\varepsilon_{w,i}$ is the strain of the ith layer of web.

The bilinear kinematic hardening model was chosen as the constitutive relation of strain and stress for the steel component and the reinforcement, and the nonlinear elastoplastic model (Hognestad model) was used for the concrete in compression to provide the stress (f_c) versus strain (ε_c) relation, as shown in Eq. (1). The contribution of the concrete tension part to the flexural strength was ignored.

Based on the strain-stress relations of the concrete and steel, the stress at each layer can be obtained. Next, the resultant force is computed by multiplying the stress by the related cross-sectional area. All the sectional forces should meet the equilibrium condition, as shown in the following equation:

$$\sum F_x = C_c + C_{tf} + C_{s,web} + C_{st} + T_{s,web} + T_{st} + T_{bf} \tag{5}$$

where C_c, C_{tf}, C_{st}, and $C_{s,web}$ are the compressive forces of the encased concrete, top steel flange, reinforcements, and corrugated steel web, respectively; and T_{bf}, T_{st}, and $T_{s,web}$ are the tensile forces of the bottom steel flange, reinforcements, and corrugated steel web, respectively.

Finally, the flexural strength of the PECGCSW (M_u) can be predicted as follows:

$$M_u = \sum_{i=1}^{N} C_i(d_i - h_1) + \sum_{i=1}^{N} T_i(d_i - h_1) \tag{6}$$

where h_1 is the height of the compression part for the composite section from the neutral axis to the top fiber, and d_i is the distance from the sectional forces C_i or T_i to the top fiber. This analytical method was confirmed by comparison with experimental results; the process details of the analysis are described in our previous investigation [36].

5.2. Shear strength

As shown in a previous experimental study of a PECGCSW subjected to shear force [34], the shear capacity of the encased concrete is considered to be controlled by tension failure in the diagonal direction on the basis of the concrete cracking pattern and strain distribution, as shown in Fig. 14. For the PECGCSW, the shear stress was distributed uniformly along the height of the steel web, and the stress achieved yielding strength at the ultimate state before the bucking of the steel web due to concrete confinement. At the same time, the concrete principal stress reached compression strength. Therefore, the shear strength, V_u, of the PECGCSW can be determined by the following equations:

$$V_u = V_{seq} + V_{ceq} \tag{7}$$

$$V_{seq} = \tau_{wy} h_w t_w / \eta \tag{8}$$

$$V_{ceq} = \beta f_c b_e t_{ceq} \sin\theta \tag{9}$$

$$\sin\theta = h_w / \sqrt{h_w^2 + L^2} \tag{10}$$

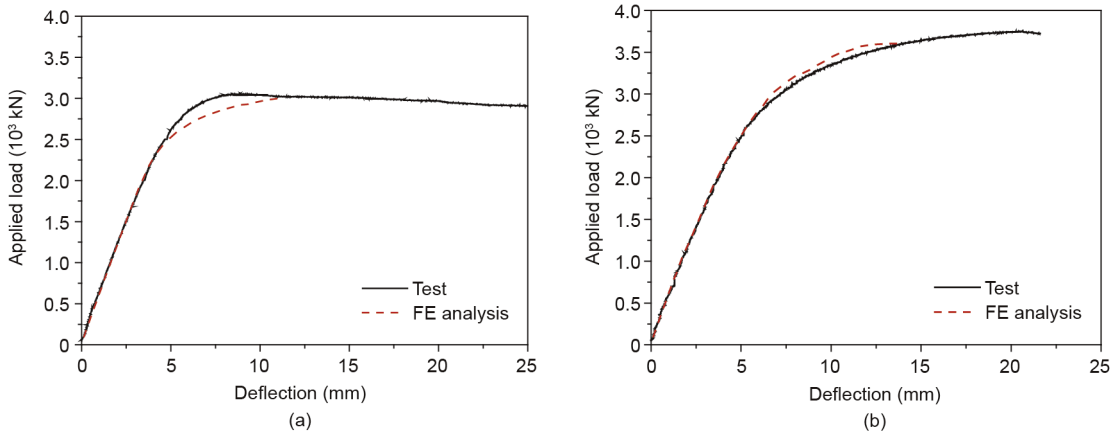

Fig. 12. Load-deflection relationships obtained from tests and FE analysis. (a) SBC1; (b) SBC2.

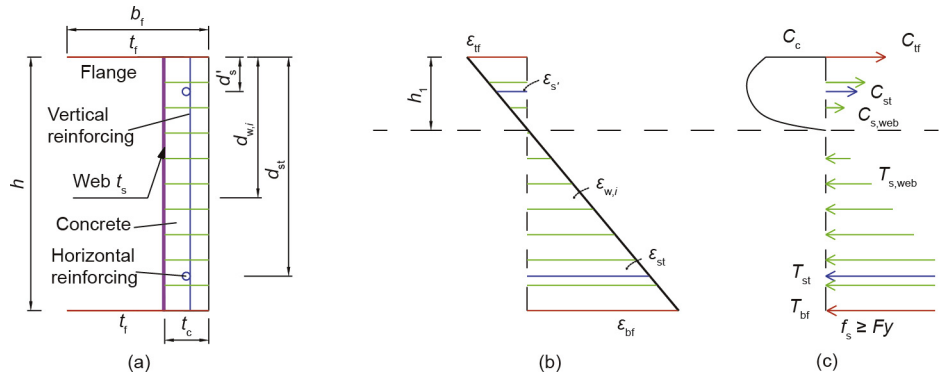

Fig. 13. The sectional strain and stress distribution of the multi-layer model in the vertical direction under the ultimate state. (a) Cross-section; (b) strain distribution; (c) stress distribution and resultant force.

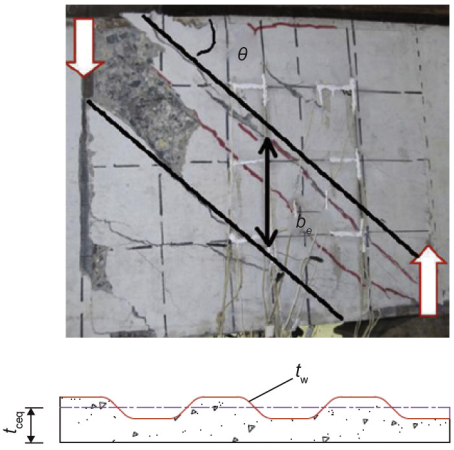

Fig. 14. The shear failure model of the PECGCSW.

$$b_e = K_e h_w \tag{11}$$

where V_{ceq} and V_{seq} represent the shear resistance provided by the concrete and corrugated web, respectively; τ_{wy}, h_w, and t_w are the yielding shear stress, height, and thickness of the corrugated steel web, respectively; t_{ceq} is the mean thickness of the concrete; the coefficient β is proposed in order to consider the non-uniform distribution of diagonal compressive stress along the concrete thickness, and is assumed to be 0.5 to be on the safe side; f_c is the concrete compressive strength; the parameter θ is the angle of the diagonal line in the shear panel; η is used to consider the corrugation effect, which is the ratio of the expanded length of one corrugation to its projected length; L is the shear span; and K_e is a ratio of the effective web height (b_e) to the actual web height, and is set to 0.3.

The accuracy and effectiveness of the shear strength prediction for the PECGCSW was also verified by experimental and numerical results from our previous work [34,35].

5.3. Interaction of flexural and shear strength

In order to evaluate the load-carrying capacity and establish the interaction curve of the PECGCSW under combined loads of shear force and bending moment, parametrical analyses using verified FE models were carried out based on experimental specimens, specimen height changes from 0.5 m to 0.8 m, and the ratio of span to height changes from 0.6 to 2.5 (L/h = 0.6–2.5), while the other parameters were kept the same as for the test specimens.

On the basis of experimental results and parametric analytical results, the interaction curve of the shear force and bending moment was investigated. In general, it is accepted that the load-carrying capacity can be determined using the theoretical flexural strength (M_u) when a PECGCSW is subjected to a pure bending moment or to a relatively small shear force that can be neglected, whereas the load-carrying capacity can be calculated by the theoretical shear strength (V_u) when a PECGCSW is subjected to a pure shear force or to a relatively small bending moment, which can be neglected. Under combined loads of shear force (V) and bending moment (M), the relationship between the dimensionless ratios of M/M_u and V/V_u was assumed to be nonlinear (power function). As shown in Eq. (12), a and b are the limits for the loading capacity calculated individually by flexural or shear strength, and c is the interaction factor.

$$\begin{cases} \frac{V}{V_u} \leqslant 1 & 0 \leqslant \frac{M}{M_u} < a \\ \left(\frac{M}{M_u}\right)^c + \left(\frac{V}{V_u}\right)^c \leqslant 1 & a \leqslant \frac{M}{M_u} \leqslant 1, b \leqslant \frac{V}{V_u} \leqslant 1 \\ \frac{M}{M_u} \leqslant 1 & 0 \leqslant \frac{V}{V_u} < b \end{cases} \tag{12}$$

Fig. 15 illustrates the load-carrying capacity prediction models under combined loads of shear force and bending moment according to experimental and numerical results. Only two test results (SBC1 and SBC2) are included in the present study. In addition, the interaction diagram of M-V for corrugated steel web girders, as proposed by Kuchta [30], is presented for comparison. The mag-

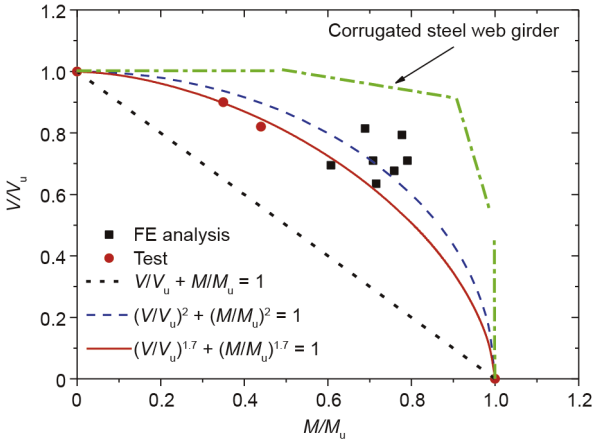

Fig. 15. Interaction curves of flexural and shear strength.

nitude of a and b were fitted as 0.1 and 0.1, respectively, indicating that when $0 \leq M/M_u < 0.1$, the load-carrying capacity is controlled by shear strength; when $0 \leq V/V_u < 0.1$, the load-carrying capacity is controlled by flexural strength; and when $M/M_u \geq 0.1$ and/or $V/V_u \geq 0.1$, the interaction of shear and bending must be considered. The average value of the interaction factor c was fitted to be 2, and the lower limit value of c was fitted to be 1.7. To be on the safe side, the lower limit value of c was suggested in order to consider the interaction between shear and bending. Since only two specimens were covered in the experimental results of the present test, the proposed curves need to be modified by more experimental data in the future.

For the purpose of practical design, the cross-sections at the end supports of a simply supported CGCSW can be designed to consider pure shear force, whereas the sections at the middle supports for a continuous girder must be designed to consider the interaction of the shear force and bending moment.

6. Conclusions

This study experimentally and analytically investigated the PECGCSW under combined shear force and bending moment. The following conclusions were drawn from this study:

(1) Experimental phenomena indicated that both flexural and shear cracking appeared on the surface of the encased concrete, resulting in obvious coupled flexural and shear failures. For specimen SBC1, with $R = 0.355$, one flexural and one shear crack occurred at the initial cracking stage. Next, as the applied load increased, shear cracks rapidly developed and finally controlled the failure mode. For specimen SBC2, with $R = 0.495$, a flexural crack first appeared at the initial cracking stage. Next, flexural cracks propagated with load increase, and shear cracks occurred gradually. Finally, flexural cracking controlled the failure mode.

(2) The R slightly affected the shear stiffness of the test specimens at the elastic stage. The shear stiffness decreased after concrete cracking; moreover, the shear stiffness of the specimen with a larger R decreased more rapidly. In addition, with an increase of R, the initial cracking load was reduced but the whole ductility was enhanced.

(3) On the basis of experimental and numerical results, interaction curves of flexural and shear strength were proposed in order to evaluate the load-carrying capacity. When $0 \leq M/M_u < 0.1$, the load-carrying capacity can be determined individually by shear strength; when $0 \leq V/V_u < 0.1$, the load-carrying capacity can be calculated only by flexural strength; and when $M/M_u \geq 0.1$ and/or $V/V_u \geq 0.1$, the interaction of the shear force and bending moment must be considered, and an interaction factor of 1.7 is suggested in order to be on the safe side.

(4) This experimental study only considers the influence of different shear span lengths on the interaction of the flexural and shear strength, and the number of specimens is limited. More experimental specimens with different cross-sections (i.e., T-shaped and box-shaped), variable cross-section heights, and so on, under combined loads of shear force and bending moment, should be tested further in order to verify and modify the load-carrying capacity evaluation of PECGCSWs.

Acknowledgements

The authors gratefully thank the National Natural Science Foundation of China (51308070, 51408070, and 51378080), the National Basic Research Program of China (2015CB057702), the Key Discipline Fund of Creative Project of Bridge and Tunnel Engineering (13ZDXK04) from the Changsha University of Science and Technology, the Open Fund of the Hunan Province University Key Laboratory of Bridge Engineering (13KA04), and the Applied Basic Research Program of Shanxi Province for their support.

Compliance with ethics guidelines

Jun He, Sihao Wang, Yuqing Liu, Zhan Lyu, and Chuanxi Li declare no conflict of interest or financial conflicts to disclose.

References

[1] He J, Chen A, Liu Y. Analysis on structural system and mechanical behavior of box girder bridge with corrugated steel webs. Proceedings of the 3rd International Conference on Steel and Composite Structures; 2007 Jul 30–Aug 1; Manchester, UK. p. 489–94.
[2] He J, Liu Y, Chen A, Yoda T. Mechanical behavior and analysis of composite bridges with corrugated steel webs: State-of-the-art. Int J Steel Struct 2012;12(3):321–38.
[3] Jiang RJ, Au FTK, Xiao YF. Prestressed concrete girder bridges with corrugated steel webs: Review. J Struct Eng 2015;141(2):04014108.
[4] Cheyrezy M, Combault J. Composite bridges with corrugated steel webs—Achievements and prospects. IABSE Rep 1990;60:479–84.
[5] Elgaaly M, Seshadri A, Hamilton RW. Bending strength of steel beams with corrugated webs. J Struct Eng 1997;123(6):772–82.
[6] Huang L, Hikosaka H, Komine K. Simulation of accordion effect in corrugated steel web with concrete flanges. Comput Struct 2004;82(23–26):2061–9.
[7] Oh JY, Lee DH, Kim KS. Accordion effect of prestressed steel beams with corrugated webs. Thin Wall Struct 2012;57:49–61.
[8] Luo R, Edlund B. Buckling analysis of trapezoidally corrugated panels using spline finite strip method. Thin Wall Struct 1994;18(3):209–24.
[9] Johnson RP, Cafolla J, Bernard C. Corrugated webs in plate girders for bridges. P I Civil Eng—Struct B 1997;122(2):157–64.
[10] Abbas HH. Analysis and design of corrugated web I-girders for bridges using high performance steel [dissertation]. Bethlehem: Lehigh University; 2003.
[11] Sayed-Ahmed EY. Design aspects of steel I-girders with corrugated steel webs. Electron J Struct Eng 2007;7:27–40.
[12] Metwally AE, Loov RE. Corrugated steel webs for prestressed concrete girders. Mater Struct 2003;36(2):127–34.
[13] Mo YL, Jeng CH, Krawinkler H. Experimental and analytical studies of innovative prestressed concrete box-girder bridges. Mater Struct 2003;36(2):99–107.
[14] Kim KS, Lee DH, Choi SM, Choi YH, Jung SH. Flexural behavior of prestressed composite beams with corrugated web: Part I. Development and analysis. Compos Part B: Eng 2011;42(6):1603–16.
[15] Elamary A, Ahmed MM, Mohmoud AM. Flexural behaviour and capacity of reinforced concrete-steel composite beams with corrugated web and top steel flange. Eng Struct 2017;135(15):136–48.
[16] Elgaaly M, Hamilton RW, Seshadri A. Shear strength of beams with corrugated webs. J Struct Eng 1996;122(4):390–8.
[17] Mizuguchi K, Ashiduka K, Yoda T, Sato K, Sakurada M, Hidaka S. Loading tests of Hondani Bridge. Bridge Found Eng 1998;32(10):25–34. Japanese.
[18] Luo R, Edlund B. Shear capacity of plate girders with trapezoidally corrugated webs. Thin Wall Struct 1996;26(1):19–44.
[19] Driver RG, Abbas HH, Sause R. Shear behavior of corrugated web bridge girders. J Struct Eng 2006;132(2):195–203.
[20] Yi J, Gil H, Youm K, Lee H. Interactive shear buckling behavior of trapezoidally corrugated steel webs. Eng Struct 2008;30(6):1659–66.
[21] Sause R, Braxtan TN. Shear strength of trapezoidal corrugated steel webs. J Constr Steel Res 2011;67(2):223–36.
[22] He J. Mechanical performance and design method of composite bridge with corrugated steel webs. Shanghai: Tongji University; 2011. Chinese.
[23] Japan Society of Civil Engineers. Design manual for PC bridges with corrugated steel webs. Tokyo: Research Committee for Hybrid Structures with Corrugated Steel Webs; 1998. Japanese.
[24] EN 1993-1-5. Eurocode 3—Design of steel structures—Part 1–5: Plated structural elements. European standard. Brussels: European Committee for Standardization; 2006.
[25] Mo YL, Jeng CH, Chang YS. Torsional behavior of prestressed concrete box-girder bridges with corrugated steel webs. ACI Struct J 2000;97(6):849–59.
[26] Mo YL, Fan YL. Torsional design of hybrid concrete box girders. J Bridge Eng 2006;11(3):329–39.
[27] Ding Y, Jiang KB, Liu YW. Nonlinear analysis for PC box-girder with corrugated steel webs under pure torsion. Thin Wall Struct 2012;51:167–73.
[28] Kadotani T, Aoki K, Yamanobe S. Vibration characteristics of corrugated steel web bridge: 1. Test. J Prestressed Concrete 2003;45(2):90–9. Japanese.
[29] Takaki Y, Fujita M, Mashiko H. Vibration characteristics of extrodosed bridges with corrugated steel webs Research Report. Tokyo: Sumitomo Mitsui Construction Co., Ltd.; 2004. p. 53–8. Japanese.
[30] Kuchta K. Zum Einfluß der Interaktion von Biegemoment und Ouerkraft auf das Tragverhalten von Wellstegträgern. Stahlbau 2006;75(7):573–7. German.

[31] Kosa K, Awane S, Uchino H, Fujibayashi K. Ultimate behavior of prestressed concrete bridge with corrugated steel webs using embedded connection. J Jpn Soc Civil Eng Ser E1 2006;62(1):202–20. Japanese.
[32] Shitou K, Nakazono A, Suzuki N, Nagamoto N, Asai H. Experimental research on shear behavior of corrugated steel web bridge. J Jpn Soc Civil Eng, Ser A1 2008;64(2):223–34. Japanese.
[33] Chen XC. Full-range behaviour of prestressed concrete bridges with corrugated steel webs [dissertation]. Hong Kong: The University of Hong Kong; 2016.
[34] He J, Liu YQ, Chen AR, Yoda T. Shear behavior of partially encased composite I-girder with corrugated steel web: Experimental study. J Constr Steel Res 2012;77:193–209.
[35] He J, Liu YQ, Lin ZF, Chen AR, Yoda T. Shear behavior of partially encased composite I-girder with corrugated steel web: numerical study. J Constr Steel Res 2012;79:166–82.
[36] He J, Liu YQ, Chen AR, Wang D, Yoda T. Bending behavior of concrete-encased composite I-girder with corrugated steel web. Thin Wall Struct 2014;74:70–84.
[37] Ollgaard JG, Slutter RG, Fisher JW. Shear strength of stud connectors in lightweight and normal weight concrete. AISC Eng J 1971;8:55–64.
[38] American Association of State Highway and Transportation Officials (AASHTO). AASHTO LRFD bridge design specifications. 3rd ed. Washington, DC: AASHTO; 2004.